SUBMITTED TO APJL MAY 11, 1998
Preprint typeset using LATEX style emulateapj

COSMIC COMPLEMENTARITY: PROBING THE ACCELERATION OF THE UNIVERSE

MAX TEGMARK[1,2], DANIEL J. EISENSTEIN[1], WAYNE HU[1] AND RICHARD G. KRON[3]

Submitted to ApJL May 11, 1998

ABSTRACT

We assess the accuracy with which Ω_m and Ω_Λ can be measured by combining various types of upcoming experiments. Useful expressions for the Fisher information matrix are derived for classical cosmological tests involving luminosity (*e.g.*, SN Ia), angular size, age and number counts. These geometric probes are found to be quite complementary both to each other and to inferences from cluster abundance and the cosmic microwave background (CMB). For instance, a joint analysis of SN Ia and CMB reduces the error bars on Ω_Λ by about an order of magnitude compared to a separate analysis of either data set.

Subject headings: galaxies: statistics — supernovae: general — large-scale structure of universe — CMB

1. INTRODUCTION

It may be possible to measure cosmological parameters with great accuracy using upcoming cosmic microwave background (CMB) experiments (Jungman *et al.* 1996; Bond *et al.* 1997; Zaldarriaga *et al.* 1997), galaxy surveys (Tegmark 1997; Goldberg & Strauss 1998; Hu *et al.* 1998) and supernova Ia (SN Ia) searches (Goobar & Perlmutter 1995; Perlmutter *et al.* 1998; Garnavich *et al.* 1998). However, no single type of measurement alone can constrain all parameters, as it will inevitably suffer from so-called *degeneracies* in which particular combinations of changes in parameters leave the result essentially unaffected (Bond *et al.* 1994, 1997; Zaldarriaga *et al.* 1997; Metcalf & Silk 1998; Huey *et al.* 1998). Fortunately, different types of cosmological measurements are often highly complementary, breaking each other's degeneracies and combining to give much more accurate measurements than any one could give alone. For example, CMB measurements are highly complementary to both galaxy surveys (Tegmark *et al.* 1997; Hu *et al.* 1998; Gawiser & Silk 1998; Webster *et al.* 1998; Eisenstein *et al.* 1998) and SN Ia (Zaldarriaga *et al.* 1997; Tegmark 1997; White 1997).

The topic of this *Letter* is probes of the acceleration of the Universe, given by the density parameters Ω_m for matter and Ω_Λ for vacuum density (cosmological constant). Most of the cosmological tests that we discuss are well-known. Our focus is on their degeneracy structure, *i.e.*, on which ones are complementary and which ones act as independent cross-checks of one another. We address this by computing the *Fisher information matrix* $\mathbf{F}$ for each of the tests. This has the advantage of explicitly showing how the accuracy and degeneracy depends on the survey details. It also allows a unified treatment of all tests, since if independent experiments are analyzed jointly, their Fisher information matrices simply add.

[1] Institute for Advanced Study, Princeton, NJ 08540; max@ias.edu, eisenste@ias.edu, whu@ias.edu

[2] Hubble Fellow

[3] FNAL, MS 127, Batavia, IL 60510

2. CALCULATION OF THE FISHER MATRICES

All data sets discussed below consist of a vector $\mathbf{x}$ of measured numbers $x_1, ..., x_N$ whose probability distribution $f(\mathbf{x};\boldsymbol{\Theta})$ depends on a vector of cosmological parameters $\boldsymbol{\Theta}$ that we wish to estimate. In our case, $\theta_1 = \Omega_m$ and $\theta_2 = \Omega_\Lambda$. The *Fisher information matrix* for a data set (see Tegmark *et al.* 1997 for a comprehensive review), defined as

$$\mathbf{F}_{ij} \equiv -\left\langle \frac{\partial^2 \ln f}{\partial\theta_i \partial\theta_j} \right\rangle, \qquad (1)$$

quantifies its information content about these parameters. Its inverse $\mathbf{F}^{-1}$ gives the best attainable covariance matrix for the measurement errors on these parameters, illustrated by the error ellipses in Fig. 2. We will now specify probability distributions f for the various cosmological tests and compute the corresponding Fisher matrices.

2.1. *Luminosity, size, age and clustering*

The cosmological tests based on luminosity, angular size, age and clustering (see *e.g.* Weinberg 1972, hereafter W72; Peebles 1993), can all be described as noisy measurements of some quantities x_n at redshifts z_n, $n = 1, ..., N$. We model them as

$$x_n = a \ln d(z;\Omega_m,\Omega_\Lambda) + b + \varepsilon_n, \qquad (2)$$

where a and b are constants independent of Ω_m and Ω_Λ, the function d incorporates the effects of cosmology and ε_n is a random term with zero mean ($\langle\varepsilon_n\rangle = 0$) including all sources of measurement error.

For luminosity tests like SN Ia, x_n is the observed magnitude of the n^{th} object and d is the luminosity distance (W72):

$$d_{lum} = (1+z)\frac{S(\kappa\eta)}{\kappa}, \quad \eta(z;\Omega_m,\Omega_\Lambda) = \int_0^z \frac{dz'}{E(z')}, \qquad (3)$$

$$E(z) \equiv \left[(1+z)^2(1+\Omega_m z) - z(2+z)\Omega_\Lambda\right]^{1/2}, \qquad (4)$$

where $\kappa \equiv \sqrt{|1-\Omega_m-\Omega_\Lambda|}$. We recognize $E = H(z)/H_0$ as the relative expansion rate at an earlier time and $1/H_0\kappa$

as (the magnitude of) the current radius of curvature of the Universe. From the definition of magnitudes, $a = 5/\ln 10$. The errors ε_n include errors in extinction correction and intrinsic scatter in the "standard candle" luminosity.

For tests involving the observed angular sizes θ_n of objects at redshifts $z_1, ..., z_N$, we define $x_n \equiv \ln\theta_n$, $a = -1$ and take d to be the the angular size distance (W72): $d_{ang} = d_{lum}/(1+z)^2$. For such tests (see *e.g.* Daly 1998; Pen 1997), ε_n includes scatter in the "standard yardstick" size.

For tests involving estimates t_n of the age of the Universe at redshifts z_n, we define $x_n \equiv \ln H_0 t_n$. Setting $a = 1$, this gives (W72)

$$d_{age} = \int_z^\infty \frac{dz'}{(1+z')E(z')}. \tag{5}$$

For tests involving the observed growth G_n in the amplitude of linear density fluctuations since redshift z_n, we choose $x_n \equiv -\ln G_n$, $a = 1$ and take d to be the linear growth factor (W72):

$$d_{gr} \equiv \frac{D(z)}{D(0)}, \quad D(z) \propto E(z)\int_z^\infty \frac{(1+z)}{E(z)^3}dz. \tag{6}$$

Assuming that the errors ε_n have a Gaussian distribution, the Fisher matrix is given by (Tegmark *et al.* 1997)

$$\mathbf{F}_{ij} = \frac{1}{2}\mathrm{tr}\left[\mathbf{C}^{-1}\mathbf{C}_{,i}\,\mathbf{C}^{-1}\mathbf{C}_{,j}\right] + \boldsymbol{\mu}_{,i}^t\,\mathbf{C}^{-1}\boldsymbol{\mu}_{,j}\,, \tag{7}$$

where $\boldsymbol{\mu} \equiv \langle\mathbf{x}\rangle$ is the mean $[\mu_n = \ln d(z_n)]$ and $\mathbf{C} \equiv \langle\mathbf{x}\mathbf{x}^t\rangle - \boldsymbol{\mu}\boldsymbol{\mu}^t$ is the covariance matrix of $\mathbf{x}$. Commas denote derivatives, so $\boldsymbol{\mu}_{,i} \equiv \partial\boldsymbol{\mu}/\partial\theta_i$. For simplicity, we will assume that

$$\mathbf{C}_{mn} = \delta_{mn}\sigma_n^2, \tag{8}$$

i.e., that all the magnitude errors ε_n are uncorrelated. Our treatment below is readily generalized to non-diagonal error models $\mathbf{C}$, more appropriate for describing systematics. Since $\mathbf{C}_{,i} = 0$, all the information about Ω_m and Ω_Λ comes from the second term in equation (7), giving

$$\mathbf{F}_{ij} = a^2\sum_{n=1}^N \frac{1}{\sigma_i^2}\frac{\partial\ln d}{\partial\theta_i}(z_n)\frac{\partial\ln d}{\partial\theta_j}(z_n). \tag{9}$$

2.2. *A supernova example*

To bring out the physics, let us evaluate this explicitly for the SN Ia example — the other cases are analogous. SN Ia have had their accuracy assessed previously, first by Goobar & Perlmutter (1995) and subsequently by making χ^2-fits to real data (Perlmutter *et al.* 1998; Garnavich *et al.* 1998; White 1998); however, this is the first treatment involving their Fisher matrix.

In this illustration, we take all magnitude errors to be equal, $\sigma_i = \Delta m$. It is instructive to rewrite equation (9) as

$$\mathbf{F}_{ij} = \frac{N}{(\Delta m)^2}\int_0^\infty g(z)w_i(z)w_j(z)dz, \tag{10}$$

where

$$w_i(z) \equiv \frac{5}{\ln 10}\left\{\frac{\kappa S'[\kappa\eta(z)]}{S[\kappa\eta(z)]}\left[\frac{\partial\eta}{\partial\theta_i} - \frac{\eta(z)}{2\kappa^2}\right] + \frac{1}{2\kappa^2}\right\}, \tag{11}$$

$$\frac{\partial\eta}{\partial\Omega_m}(z) = -\frac{1}{2}\int_0^z \frac{z'(1+z')^2}{E(z')^3}dz', \tag{12}$$

$$\frac{\partial\eta}{\partial\Omega_\Lambda}(z) = \frac{1}{2}\int_0^z \frac{z'(2+z')}{E(z')^3}dz', \tag{13}$$

and the SN Ia redshift distribution is given by $g(z) = \frac{1}{N}\sum_{n=1}^N \delta(z - z_n)$. The expression in braces approaches

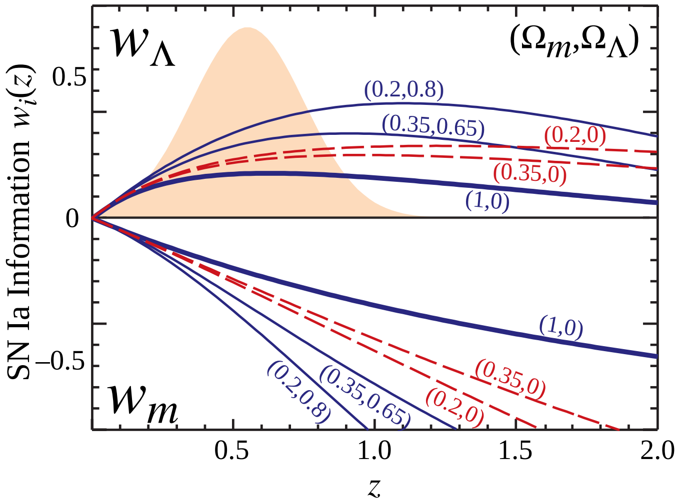

FIG. 1 — The SN Ia weight functions w_Λ (positive) and w_m (negative) are plotted for standard CDM, two open ($\Omega_\Lambda = 0$) models and two flat ($\Omega_\Lambda = 1 - \Omega_m$) models. The Fisher matrix element $\mathbf{F}_{ij}$ is computed by simply integrating the product of the curves w_i and w_j and a redshift distribution f such as the shaded one.

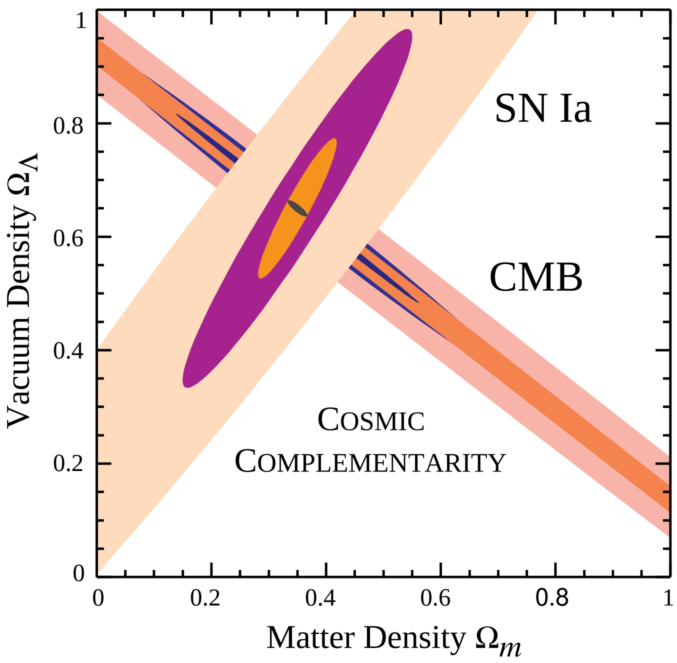

FIG. 2 — 68% confidence regions are shown for the upcoming CMB experiments and hypothetical SN Ia data sets specified in Table 1. The assumed fiducial model is COBE-normalized ΛCDM with $\Omega_m = 0.35$, $\Omega_\Lambda = 0.65$, $\Omega_b = 0.05$, and $h = 0.65$. Combining the CMB and SN Ia data shrinks the error region to the overlap of the two corresponding ellipses: for instance, a joint analysis of the optimistic SN Ia case with polarized Planck data gives the tiny black ellipse in the center.

$\eta^{-1}\partial\eta/\partial\theta_i - \eta^2/6$ as $\kappa \to 0$. The contribution to $\mathbf{F}$ from each redshift can thus be split into two factors, one reflecting the quality of the data set ($Ng[z]/\Delta m^2$) and the other incorporating the effects of cosmology (the weight functions w_i). The functions w_i are plotted in Figure 1 for a variety of cosmological models.

If all the observed supernovae were at the same redshift z, then the resulting 2×2 Fisher matrix $\mathbf{F}_{ij} \propto w_i(z)w_j(z)$ would have rank 1, *i.e.*, be singular. The vanishing eigenvalue would correspond to the eigenvector $(w_\Omega, -w_\Lambda)$. Physically, this is because there is more than one way of fitting a single measured quantity $d_{lum}(z)$ by varying two parameters (Ω_m and Ω_Λ). The corresponding ellipse in Figure 2 would be infinitely long, with slope $-w_\Omega/w_\Lambda$, the ratio of the magnitudes of the Ω_m and Ω_Λ curves in Figure 1 at that redshift. The SN Ia ellipses plotted in Figure 2 correspond to a range of redshifts, with f being a Gaussian of mean $\bar{z}$ and standard deviation Δz given by Table 1. This breaks the degeneracy only marginally, leaving the SN ellipses quite skinny, since the ratios w_Ω/w_Λ in Figure 1 are seen to vary only weakly with z.

2.3. *Counts*

For a sample of objects volume limited out to redshift z_{max}, the average number per unit redshift is (W72)

$$p(z) \propto \frac{d_{lum}(z)^2}{(1+z)^2 E(z)}. \qquad (14)$$

Defining $x_i = z_i$, the probability distribution for the observed set of N redshifts $\mathbf{x}$ is not a multivariate Gaussian as above, but a multivariate Poisson distribution,

$$f(\mathbf{x}) = e^{-\bar{N}}\frac{\bar{N}^N}{N!}\prod_{n=1}^{N} g(z_n), \qquad (15)$$

where $\bar{N} \equiv \langle N\rangle = \int_0^{z_{max}} p(z)dz$ is the expected number of objects and $g(z) \equiv p(z)/\bar{N}$ can be interpreted as a probability distribution for the redshift of a typical object. Note that the integer N is itself random, with a Poisson distribution. Substituting equations (14) and (15) into (1) gives

$$\mathbf{F}_{ij} = -\bar{N}\int_0^{z_{max}} \frac{\partial^2 \ln g}{\partial\theta_i\partial\theta_j} g(z)dz + \frac{1}{\bar{N}}\frac{\partial\bar{N}}{\partial\theta_i}\frac{\partial\bar{N}}{\partial\theta_j}. \qquad (16)$$

We will neglect the last term to be conservative, since it reflects the information coming from the (*a priori* unknown) overall normalization.

3. ACCURACY AND DEGENERACY

How do these tests compare with regard to accuracy and degeneracy? Their degeneracy structure is illustrated in Figure 3, which shows contour plots of d_{lum}, d_{lum}^2/E, t, and $D/D(0)$ at three redshifts. Using objects at a single redshift z, a test is unable to distinguish between models lying along the same contour curve. The luminosity and size tests have identical degeneracy structure because both probe $S(\kappa\eta)/\kappa$; their degeneracy curves are seen to rotate anti-clockwise from a slope of $1/2$ (explained below in §) at $z=0$ to negative at $z=\infty$. The count contours rotate in the same sense as z increases. The isochrones rotate similarly but have a richer structure at $z=0$ because the age of the Universe probes E at all redshifts. They become vertical at high redshift where the age is independent of Ω_Λ. The growth factor degeneracy curves are seen to have a slope steeper than -1 in most of our parameter space. This is because increasing the hyperbolic curvature $1-\Omega_m-\Omega_\Lambda$ makes fluctuation growth freeze out earlier, increasing $D(z)/D(0)$, and increasing Ω_Λ at fixed curvature typically has the same effect. The evolution of cluster abundance places powerful constraints on $D(z)/D(0)$ (Bahcall & Fan 1998). Although this test gives highly non-Gaussian errors ε_n (the constraints are mainly one-sided), its degeneracy structure is still given by Fig. 3.

The list of geometry tests that we have discussed is far from complete. For instance, nonlinear effects in weak lensing (Jain & Seljak 1997) and strong lensing (Falco *et al.* 1998; Bartelmann *et al.* 1998) are promising probes of Ω_m and Ω_Λ. With CMB fixing other parameters, baryonic features detected in future galaxy redshift surveys would give fairly vertical degeneracy curves, potentially measuring Ω_m to percent levels (Eisenstein *et al.* 1998).

For all tests modeled above, the *size* of the error ellipses scales as $\sigma/\sqrt{N}$, whereas the *shape* (slope and eccentricity) is given by the degeneracy structure. The CMB ellipses in Figure 2 have been computed as in Eisenstein *et al.* (1998), marginalizing over 10 additional parameters. This CMB information on Ω_m and Ω_Λ comes mainly from the angular location of acoustic features in the power spectrum, which depends principally on the curvature term κ, *i.e.*, on the combination $\Omega_m+\Omega_\Lambda$.

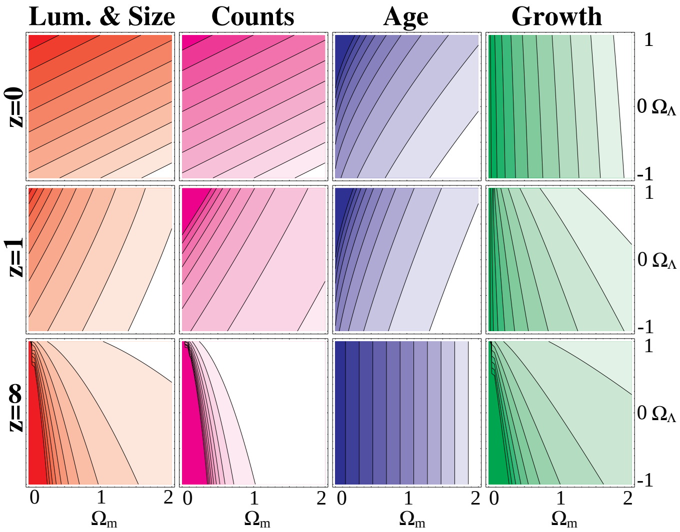

FIG. 3 — How the degeneracy structure of different cosmological tests rotates with redshift. All 12 panels have same axes.

3.1. *Low redshift observations such as SDSS*

It is well known that if data is available only for $z \ll 1$, then to first order, the luminosity, angle and count tests probe only the parameter combination $q_0 \equiv \Omega_m/2 - \Omega_\Lambda$. In this limit, our results reduce to

$$\mathbf{F} = \begin{pmatrix} 1/4 & -1/2 \\ -1/2 & 1 \end{pmatrix} (\Delta q_0)^{-2}, \qquad (17)$$

where $\Delta q_0 = 2\ln 10\Delta m/5N^{1/2}z_{rms}$ for luminosity tests using objects at rms redshift of z_{rms} with magnitude errors Δm, $\Delta q_0 = 2\sigma/N^{1/2}z_{rms}$ for corresponding angular size tests on objects with fractional size errors σ, and $\Delta q_0 = 2(5/3\bar{N})^{1/2}/z_{max}$ for number count tests volume limited to z_{max}. This is why the corresponding $z = 0$ panels in Figure 3 both give the same slope 1/2.

Because of this scaling, the huge number of galaxies in upcoming surveys such as SDSS and 2dF may allow them to place competitive constraints on q_0, as shown in Table 1, despite being a factor of several below SN Ia in redshift. Here we have assumed that fitting a Schechter luminosity function to N galaxies at the same redshift determines the parameter L_* to within $5/N^{1/2}$ magnitudes, which is conservative based on Table 2 in Lin *et al.* (1996). An obvious obstacle to such measurements is that galaxy evolution (in luminosity, size and number density) can mimic a change in q_0. However, the brute force statistical power of these data sets is so large that even subsamples of 1% of the galaxies give interesting constraints. Studying how the "q_0"-estimates vary as the galaxies are subdivided by, *e.g.*, morphology, luminosity and surface brightness therefore holds the potential of providing interesting information about galaxy evolution and perhaps the true q_0.

4. CONCLUSIONS

In conclusion, we have derived useful expressions for the Fisher information matrix for a number of classical cosmological tests and combined them with the Fisher matrix of the CMB. Whereas two identical data sets give only a factor of $\sqrt{2}$ improvement in error bars when combined, the gain factor was found to exceed 10 when combining SN Ia with CMB. This "cosmic complementarity" is due to the fortuitous fact that although either data set alone suffers from a serious degeneracy problem, the directions in which they are insensitive (in which the ellipses in Figure 2 are elongated) are almost orthogonal. The complementarity is even more dramatic for a standard $\Omega_m = 1$, $\Omega_\Lambda = 0$ CDM cosmology (Tegmark *et al.* 1998), where a smaller ISW effect worsens the CMB degeneracy.

Figure 3 shows that this complementarity is rather generic, with degeneracy curves in virtually all directions. This means that when three different tests are combined, there will be an important cosmic consistency check. If three skinny ellipses fail to overlap, at least one measurement must be wrong, whereas if they all cross at the same point, even hardened sceptics are likely to be impressed.

The potential power of upcoming CMB measurements has led to a widespread feeling that they will completely dominate cosmological parameter estimation, with other types of experiments making only marginal contributions. Because of cosmic complementarity, of which the present paper gives a number of examples, this view is misleading: two data sets combined can be much more useful than either one alone.

ACKNOWLEDGMENTS

We thank David Hogg, Alex Kim, Robert Kirshner, Saul Perlmutter, Doug Richstone, Adam Riess and Martin White for useful discussions. MT was supported by NASA through grant NAG5-6034 and Hubble Fellowship HF-01084.01-96A from STScI, which is operated by AURA, Inc. under NASA contract NAS5-26555. DJE is a Frank and Peggy Taplin Member at the IAS, and WH is supported by the Keck Foundation and a Sloan Fellowship. DJE and WH are also supported by NSF-9513835.

REFERENCES

Bahcall, N. A., & Fan, X. 1998, astro-ph/9803277
Bartelmann, M. *et al.* 1998, astro-ph/9707167
Bond, J. R. *et al.* 1994, *Phys. Rev. Lett.*, **72**, 13
Bond, J. R., Efstathiou, G., & Tegmark, M. 1997, *MNRAS*, **291**, L33
Daly, R., Guerra, E. J., & Wan, L. 1998, astro-ph/9803265
Eisenstein, D. J., Hu, W., & Tegmark, M. 1998, in preparation
Falco, E. E., Kochanek, C. S., & Munoz J M 1998, astro-ph/9707032
Goldberg, D. M., & Strauss, M. A. 1998, *ApJ*, **495**, 29
Garnavich, P. M. *et al.* 1998, *ApJL*, **493**, L53
Gawiser, E., & Silk, J. 1998, in preparation.
Goldberg, D. M., & Strauss, M. A. 1998, *ApJ*, **495**, 29
Goobar, A., & Perlmutter, S. 1995, *ApJ*, **450**, 14
Hu, W., Eisenstein, D. J., & Tegmark, M. 1998, astro-ph/9712057
Huey, G. *et al.* 1998, astro-ph/980427, private communication
Jain, B., & Seljak, U. 1997, *ApJ*, **484**, 560
Jungman, G., Kamionkowski, M., Kosowsky, A., & Spergel, D. N. 1996, *Phys. Rev. D*, **54**, 1332
Lin, H. *et al.* 1996, *ApJ*, **464**, 60
Metcalf, R. B., & Silk, J. 1998, astro-ph/9708059
Peebles, P. J. E. 1993, *Principles of Physical Cosmology* (Princeton U. P.: Princeton)
Pen, U. 1997, *New. Astr.*, **2**, 309
Perlmutter, S. *et al.* 1998, *Nature*, **391**, 51
Stompor, R., & Efstathiou, G. 1998, in preparation
Tegmark, M. 1997, *Phys. Rev. Lett.*, **79**, 3806
Tegmark, M., Eisenstein, D. J., & Hu, W. 1998, astro-ph/9804168
Tegmark, M., Taylor, A. N., & Heavens, A. F. 1997, *ApJ*, **480**, 22
Webster, M. *et al.* 1998, astro-ph/9802109
Weinberg, S. 1972, *Gravitation and Cosmology* (Wiley: New York)
White, M. 1998, astro-ph/9802295
Zaldarriaga, M., Spergel, D., & Seljak, U. 1997, *ApJ*, **488**, 1

Table 1 — Attainable error bars $\Delta\Omega_i$ for various combinations of data sets. The rows correspond to using CMB alone, three forecasts (pessimistic, middle-of-the-road, and optimistic) for available SN Ia data in five years time, and the SDSS tests described in the text. The CMB columns correspond to the upcoming MAP and Planck satellite missions without (−) and with (+) polarization information. Planck+ is seen to improve over the "No CMB" column by about an order of magnitude in $\Delta\Omega_\Lambda$, and the difference is even greater between the "Opt" and "No SN" rows. The "No SN" row is overly conservative, since gravitational lensing breaks the CMB degeneracy somewhat (Metcalf & Silk 1998; Stompor & Efstathiou 1998) but this lensing information is dwarfed by the SN Ia in the other rows.

					No CMB		MAP−		MAP+		Planck−		Planck+	
Test	N	Δm	$\bar{z}$	Δz	$\Delta\Omega_m$	$\Delta\Omega_\Lambda$	$\Delta\Omega_m$	$\Delta\Omega_\Lambda$	$\Delta\Omega_m$	$\Delta\Omega_\Lambda$	$\Delta\Omega_m$	$\Delta\Omega_\Lambda$	$\Delta\Omega_m$	$\Delta\Omega_\Lambda$
No SN Ia	0	–	–	–	∞	∞	1.4	1.1	.25	.20	1.2	.96	.14	.11
Pess SN Ia	100	0.5	0.55	0.2	.52	.68	.07	.06	.07	.06	.07	.06	.06	.05
Mid SN Ia	200	0.3	0.65	0.3	.13	.21	.03	.04	.03	.03	.03	.02	.03	.02
Opt SN Ia	400	0.2	0.70	0.4	.05	.08	.02	.03	.01	.02	.01	.01	.01	.01
SDSS L_*	10^6	5	$z_{rms} = 0.1$		∞	∞	.04	.02	.03	.02	.01	.01	.005	.004
SDSS counts	5×10^5	–	$z_{max} = 0.1$		∞	∞	.05	.03	.02	.01	.03	.02	.03	.02